On the modelling of the specific energy consumption for the continuous fibre fabrication of composite materials

On the modelling of the specific energy consumption for the Continuous Fibre Fabrication of composite materials

Abstract

The use of composite materials is growing rapidly, although the manufacturing processes and the produced components require careful consideration from a life-cycle perspective. As a result of recent technological advances, the additive manufacturing (AM) of composites has attracted a great deal of industrial interest, but the environmental impact, compared to more traditional manufacturing routes, has not yet been fully explained. This research has focused on continuous fibre fabrication (CFF), a material extrusion (MEX) process that is capable of producing long-fibre reinforced components. The energy requirements of CFF have been characterised experimentally by varying the deposition conditions (such as the process parameters, component geometries, reinforcing fibres and matrix materials). A model, which separately considers the contributions of each deposited material, i.e., the reinforcing fibre or the matrix, to account for the different operating regimes of the system, has been proposed to quantify and estimate the printing energy and the specific energy consumption (SEC). Validation of the model has confirmed a satisfactory predictive capability. SEC values ranging from 17 to 23 kWh/kg (i.e., 161 to 218 MJ oil-equivalent, where a primary-to-secondary energy conversion efficiency of 0.38 was assumed) have been obtained for fibre-reinforced components. The results suggest that CFF could be energy intensive with respect to high-productivity conventional manufacturing routes, but it could be competitive compared to low-volume processes.

Keywords: Additive manufacturing; Continuous fibre fabrication; Sustainable manufacturing; Energy demand; Deposition rate

1. Introduction

There is a growing global focus on the efficient use of energy and resources [1]. According to a report by the McKinsey Global Institute [2], approximately half of all worldwide countries could have leveraged on their resource endowments for economic growth by 2023. This presents a significant opportunity for these economies to transform their prospects and avoid squandering their resources [3, 4]. Industrial and scientific communities are now paying attention to developing energy-saving manufacturing routes and implementing life cycle assessments and optimisation over a broader spectrum [5-7]. Jayal et al. [8], when accounting for the environmental responsibility of the industrial sector, emphasised the need for a shift to a 6R concept (reduce, reuse, recycle, recover, redesign, remanufacture) at the product level to promote sustainable manufacturing. The adoption of 6R strategies in manufacturing could in fact enable a transition from the linear, open-loop, single life-cycle paradigm (based on the 'take-make-use-dispose' principle) to a circular economy (CE) model, which involves recovering value from waste streams and extending product lifetimes [9]. Chen et al. [10], who contextualised the CE model within the current manufacturing paradigm, traced the shift from craft production to mass production and then to mass-customised production, culminating in the present-day direct digital manufacturing (DDM).

As far as the aerospace and automotive industries are concerned, fibre-reinforced polymers have the potential of replacing metal components, and therefore of reducing energy requirements and CO_2 emissions [1, 11]. Lightweighting systems made up of composite materials can save up to 1100 PJ annually for passenger cars and 300 PJ for aircraft [1]. However, as the use of composites increases, handling waste is becoming a growing concern, due to their complex material nature. According to Naqvi et al. [12], carbon fibre (CF) waste in high-value industries will rise from 10 to 180 thousand tonnes by 2060. Recycling techniques can be classified as mechanical, thermal, or chemical processes [13, 14]. Thermal and solvolysis methods are suitable for CF and involve less mechanical degradation than the use of glass fibres [15, 16]. Nevertheless, there is still an industrial need for manufacturing approaches for composites characterised by (*i*) high energy efficiency, and (*ii*) the minimum use of materials, concerning both those required for the process and those that have to be disposed of at the end of the product life.

The Specific Energy Consumption (*SEC*) parameter (which quantifies the amount of energy required to process a unit mass of material [17, 18]) has been identified, in terms of energy efficiency at the manufacturing process level, as one of the factors that should be considered for process optimisation and selection tools [19]. Several studies have already used *SEC* as a holistic parameter to describe a variation of the energy demand as a function of the key manufacturing process variables. For example, *SEC* has been correlated with machine throughput in injection moulding [20], the material removal rate in machining [18], the extrusion rate in friction stir extrusion [21] and the average deposition rate (DR_a) in additive manufacturing (AM) technologies [17, 22]. The data pool on the specific energy consumption needed to produce composite components, although scattered, is growing, as reviewed in Section 1.1. Currently, there is a major gap in knowledge concerning the additive manufacturing (AM) of composites (as highlighted in Section 1.2), which, however, can enable a

transition to digital manufacturing and lead to significant material savings, due to the additive nature of the process.

There is in particular a limited number of studies on predictive energy consumption models, and the aim of this work has therefore been to contribute to filling this gap by providing both the characterisation and the modelling of energy requirements of Continuous Fibre Fabrication (CFF), an AM technology that is currently available for the production of long-fibre reinforced composites. Although other works have obtained models, through design of experiments and regression analysis, which have been used to investigate the key process parameters [23], an *SEC*-based model was preferred in this research. It is worth noting that models used to quantify and/or predict energy consumption at the unit process level are particularly interesting for the optimisation of energy efficiency. They also serve as a basis for developing LCA-based decision support tools. Consequently, this type of research could find practical applications in any company whatsoever (e.g., in the aerospace or automotive sectors) where the focus is on the sustainable development of manufacturing alternatives to conventional production routes for composite materials. *SEC* has here been modelled by identifying the different stages of the process, which is facilitated by the layer-by-layer production, and considering the fibre and matrix deposition contributions separately. This approach, which takes into account multi-material deposition, also allows the modelling approaches already available in the literature for other AM processes (e.g., [17, 22]) to be extended.

1.1. SEC for the manufacturing of composites

Figure 1 provides an overview of the *SEC* values of the most commonly used composite manufacturing techniques. As can be seen, the autoclave process has the widest range of energy consumption variation [7, 24-28], while the preform matched die processes [7, 26-28], filament winding and pultrusion have the lowest energy requirements [7, 13, 26-30]. The autoclave energy demand increases for niche applications (e.g., in the aeronautic sector and for low volume production [25, 27]). Processed resin (thermoset or thermoplastic) also affects the *SEC* value [24]. The press in compression moulding is heated and the raw material is loaded at room temperature. Such techniques represent an interesting alternative to autoclave processes, from an *SEC* point of view [26, 29, 30]. Thermoforming processes show a higher *SEC* [29, 30], but which is still below that of the autoclave technology. Thermoforming technologies are characterised by the use of a cold press and hot raw materials. The difference in the *SEC* parameter for the two compression techniques is that, in thermoforming processes, the raw material is heated outside the press, which can result in energy losses. Instead, the reinforcing fibre and resin are mixed directly in the mould in cold press techniques, and no heat source is required before or during the curing [7, 27, 29, 30]. In addition, curing under pressure is carried out over a longer period of time than the previously mentioned compression techniques. The energy demand for cold diaphragm forming (CDF) is affected by the high melting point and the long curing cycle time of the processed materials [24, 31]. Injection technologies typically have lower *SEC* values and higher production rates than those based on the autoclave technology. Vacuum assisted resin injection (VARI) processes [7, 26-30] require less energy than Resin Transfer Moulding (RTM), because of their lower working pressure [7, 13,

24, 26-28]. Hand lay-up techniques [27, 29, 30] and spray-up techniques [7, 26-30] show comparable *SEC* values, because they adopt a similar approach to overlapping composite material layers. However, the spray-up process requires slightly lower values because it resorts to automated tools. Finally, there is a lack of energy consumption data for the automated fibre placement (AFP) and the automated tape laying (ATL) processes. Moreover, in reference [32], the calculated range only considered the laser input energy to the process. Therefore, a higher *SEC* could be expected if the energy demand of the other auxiliary systems were also included. There is also a lack of data on additive manufacturing techniques among the reviewed processes for composites [33]. Figure 1 summarises the main data from the above sources, with all raw data converted to MJ oil equivalents [34].

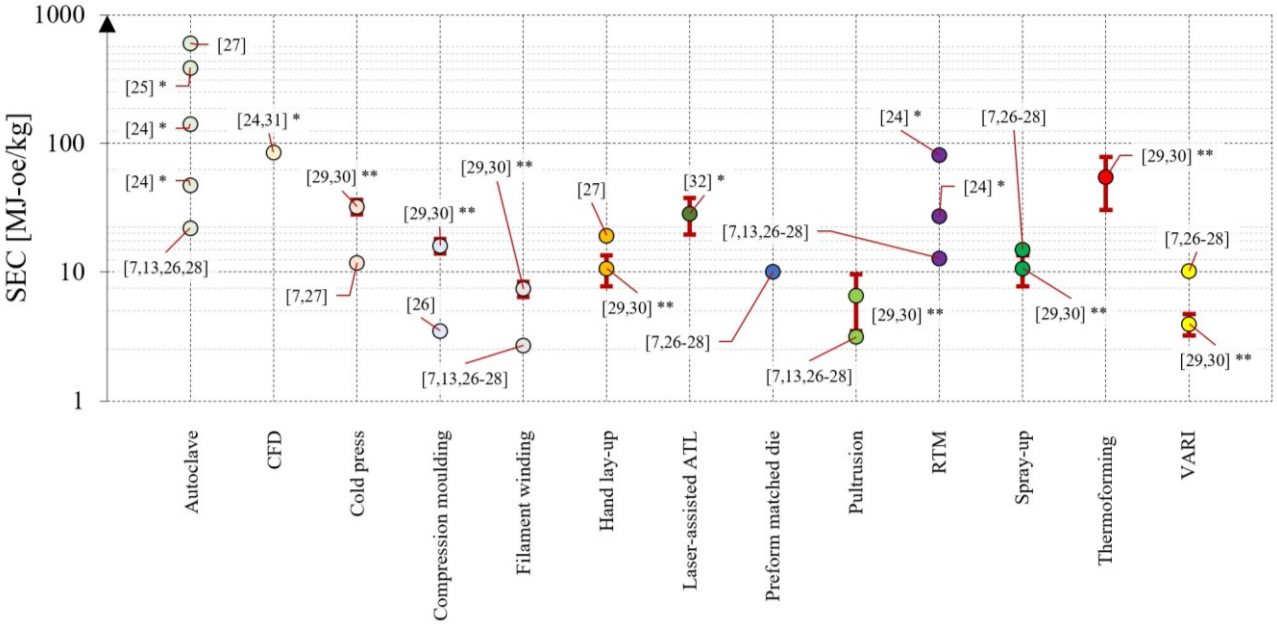

Figure 1. *SEC* data from the literature on composite manufacturing processes. Values marked with * and ** were available in kWh and primary energy intensity BTU, respectively. For consistency reasons, all the raw data were converted to MJ oil equivalents.

1.2. Additive manufacturing for composites

Additive manufacturing (AM) and AM-based hybrid processes [35, 36] are considered key drivers of the migration to DDM and have been hailed as breakthrough Industry 4.0 technologies in modern companies [37]. The publicly available information of General Electric (GE) and Avio Aero pertaining to the production of the largest civil aircraft engine, which contains more than 300 parts made by means of AM, confirms that a remarkable weight reduction can be achieved by extensively exploiting AM. GE also utilised AM to manufacture turbine blades using titanium aluminides [38]. In such an application, AM increased the productivity of the turbine blades, while reducing the component mass, compared to the previously used casting process for nickel-based alloys. Moreover, AM techniques are being recognised for their environmental impact saving potential throughout the product life-cycle [39, 40]. Paris et al. [41] compared the environmental impacts of turbines manufactured using a five-axis milling process and AM powder bed fusion with an electron beam (PBF-EB) technology, including the subsequent finishing operation, and found that PBF-EB could be a

valuable option for complex parts and that material savings could be achieved. Many AM-based technologies have been adapted for the production of composite parts to produce components reinforced with short or long fibres [33]. The powder bed fusion process utilises a low-power laser for polymers (PBF-LB/P) to sinter thermoplastic powders (e.g., PA, PE, PEEK) in a powder bed. The powder bed of composites is a mix of polymeric powder and short fibres (e.g., glass fibres, carbon particles, nanoclays or nano-Al_2O_3) [42, 43]. Three-dimensional printing (3DP) is a powder bed process that uses a polymeric binder which is selectively jetted onto a pre-deposited powder layer. Different materials can be jetted simultaneously, because of the use of multiple nozzles, while controlling the composition of the local material (e.g., epoxy resin and carbon nano-fibres) [42]. Longer fibres cannot be used in PBF-LB/P and 3DP because they can affect the flatness of the powder bed. Laminated object manufacturing (LOM) involves overlapping sheets reinforced with particulates or fibres. The composite properties can be varied by using layers of different commercial prepreg sheets or any fibre preform [42, 43]. Stereolithography (SLA) is a vat photopolymerisation process that activates a resin (e.g., epoxy or acrylic) through the use of a laser. The photopolymerisation process is then completed in a UV light oven. Reinforcing materials, such as carbon, glass and aramid fibres, can be added to create composites in the form of particles, short fibres, continuous fibres, or mats [42, 43]. Material extrusion AM (MEX) is the most flexible technique for the production of composite components. It uses a polymeric-based filament that is extruded through a heated nozzle and then deposited layer by layer. Multiple nozzles can be used to enable multi-material printing. Liquid deposition modelling (LDM) is an MEX process that uses fluid-like feedstock (e.g., epoxy resin, dimethyl methyl phosphonate) reinforced with short fibres or particles [42, 43]. Among the other processes, continuous fibre fabrication (CFF) belongs to the MEX category and is capable of producing components reinforced with long fibres, as described in Section 2. Section 3 details the experimental design and measured outcomes. The results and the *SEC* model are presented in Sections 4 and 5, respectively, while the main conclusions and perspectives for future research are summarised in Section 6.

2. Continuous Fibre Fabrication

Continuous Fibre Fabrication (CFF) is a MEX process that was developed by Markforged®. A scheme of the process is shown in Figure 2. The equipment uses a print head which has two nozzles, one for the matrix filament and one for the reinforcing fibre filament [44]. The matrix filament can be either nylon (trade name: Nylon - EoL™) or micro carbon-fibre filled nylon (Onyx™) [45]. The reinforcing fibre filament is composed of long fibres encapsulated in a polymeric matrix, which allows the fibre to be extruded through the nozzle. There are four commercially available reinforcements: carbon fibre (CF), fibreglass (FG), Kevlar (K), and high-strength high-temperature (HSHT) fibreglass. The nozzles are heated until the softening temperature of the filament is reached, and the filament is then extruded. The print head deposits the materials by moving across the XY plane, and the height of the printed layer is defined by a movement perpendicular to the print bed (across the Z direction). The reinforcing fibre filament is deposited continuously within a single layer according to a pre-defined path, which depends on the deposition strategy. Therefore, the reinforcing fibre filament is deposited onto the entire area that has to be reinforced, without interruption. When the layer has been completed, the filament is cut by means of a cutter positioned just above the nozzle. Adhesion between the reinforcing fibre filament and the previous layer or the surrounding material is ensured by the polymer matrix that encapsulates the continuous fibre.

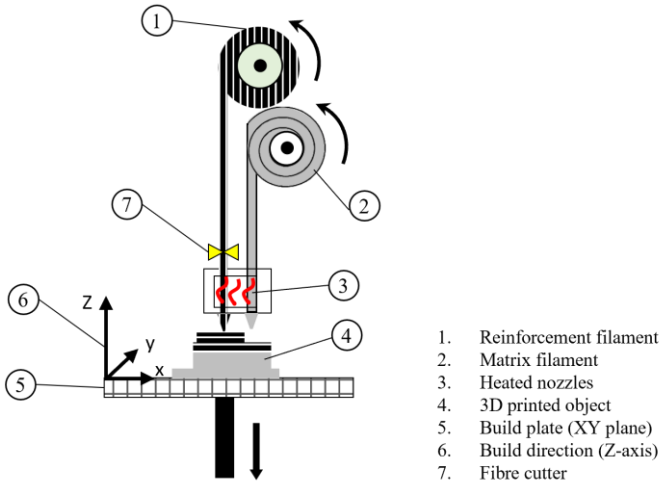

Figure 2. Simplified representation of the operational principle of the Continuous Fibre Fabrication (CFF) process.

The Eiger™ control software of the CFF machine includes only a limited number of settings pertaining to the choice of the matrix material and of the reinforcing fibre, the number of layers to be reinforced, the fibre orientation and the matrix filling strategy. Although the user can define the layer thickness of matrix-printed parts, the layer thickness of reinforced components is automatically set when the type of reinforcing fibre is selected. The layer thickness is 0.100 mm for K-reinforced parts, while it is 0.125 mm for CF-reinforced parts. The filling strategy for the matrix can be ‘triangular’, ‘hexagonal’, or ‘rectangular’, depending on the desired density of the matrix layers. Section perimeters (wall layers) are printed concentrically using the matrix filament. For unreinforced layers, the section perimeters are deposited first, followed by the filling material.

In the reinforced layers, the reinforcing filament is printed in the inner area, followed by the matrix filament for the section perimeter. An additional matrix material is deposited to fill the space left by the continuous fibre deposition. For the reinforced components, a certain amount of matrix filament is automatically purged, at the beginning of each layer, to clean the nozzle.

3. Materials and methods

The energy demand of a Markforged® MarkTwo™ machine with a build volume of 320 × 132 × 154 mm^3 was characterised. Among the available materials, both the Nylon - EoL™ and Onyx™ matrix filaments were used, while carbon fibre (CF) and Kevlar (K) were chosen as the reinforcing fibres.

3.1. Experimental plan

According to the current literature on AM, energy consumption is influenced by the complexity of the geometry that has to be printed and by the processing conditions (e.g., [17, 22]). Different geometries were designed and produced under different processing conditions to characterise the CFF process. The selected components, which are shown in Figure 3, are a flange (A), a cube (B) and two types of tensile specimens (C and D). Additive manufacturing processes are capable of producing a wide range of geometries, albeit typically in small-to-medium batches. The rationale behind the choice of the geometries considered here was to have both simple and relatively more complex parts, such as the flange and the cover used for the model validation in Section 5.4, so that any potential geometry-related differences in energy consumption could be verified.

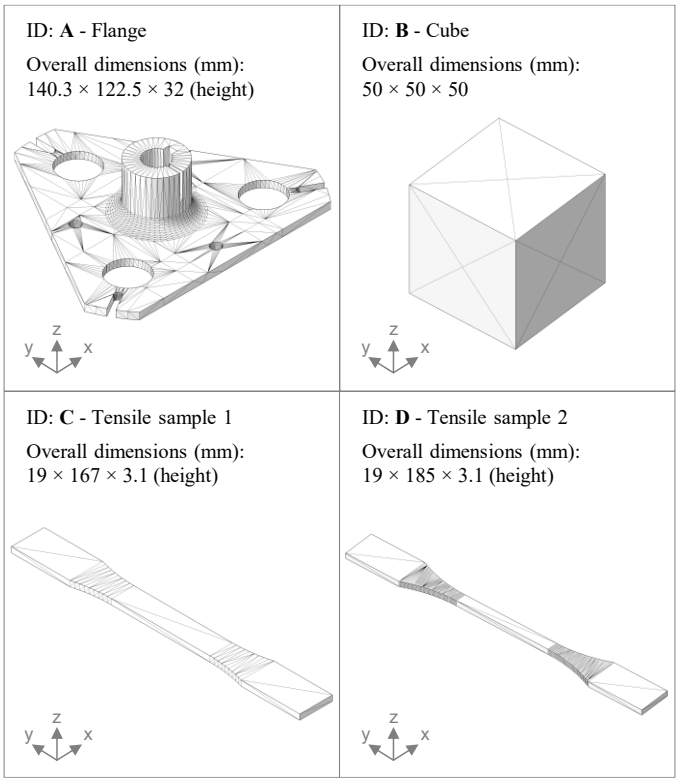

Figure 3. Components considered for the experimental tests.

As mentioned above, the Eiger™ system control limits the choice of settings. Therefore, the machine controller automatically sets the extrusion temperature to 275°C for the matrix material and 255°C for the reinforcing filament. The layer thickness could only be varied for the components printed with the matrix material, while the layer was set automatically for the reinforced ones according to the type of fibre. Therefore, the layer thickness of the components reinforced with the CF and the K fibre was fixed and equal to 0.125 mm and 0.100 mm, respectively. All the other available process settings were varied according to Table 1 and Table 2, which list the combinations of part geometries and process parameters for the unreinforced and reinforced components, respectively. Each condition is named 'Job' and is followed by a number that identifies the test. A total of 34 conditions were analysed. In consideration of all potential combinations of variables that can be set in the system control software (such as the fill pattern/density, the number of section perimeters, et cetera), this sub-set permitted the investigation of a range of deposition paths and deposition rates that is expected to be representative of the typical operating conditions of CFF in practical industrial applications, as further detailed hereafter.

Test	Geometry	Fill pattern	Fill density	Number of section perimeters	Layer thickness [mm]	Matrix material
Job 1	A	Rectangular	Solid	1	0.200	Nylon - EoL™
Job 2	A	Rectangular	Solid	1	0.100	Nylon - EoL™
Job 3	A	Rectangular	Solid	4	0.100	Nylon - EoL™
Job 4	A	Rectangular	Solid	2	0.100	Nylon - EoL™
Job 5	A	Hexagonal	30%	1	0.100	Nylon - EoL™
Job 6	A	Rectangular	Solid	1	0.200	Onyx™
Job 7	A	Rectangular	Solid	1	0.100	Onyx™
Job 8	A	Rectangular	Solid	4	0.100	Onyx™
Job 9	A	Rectangular	Solid	2	0.100	Onyx™
Job 10	A	Hexagonal	30%	1	0.100	Onyx™
Job 11	B	Rectangular	Solid	1	0.200	Nylon - EoL™
Job 12	B	Rectangular	Solid	1	0.200	Onyx™
Job 13	C	Rectangular	Solid	2	0.125	Onyx™
Job 14	C	Rectangular	80%	2	0.125	Onyx™
Job 15	C	Rectangular	50%	2	0.125	Onyx™
Job 16	C	Rectangular	30%	2	0.125	Onyx™
Job 17	C	Hexagonal	50%	2	0.125	Onyx™
Job 18	C	Hexagonal	30%	2	0.125	Onyx™
Job 19	C	Triangular	50%	2	0.125	Onyx™
Job 20	C	Triangular	30%	2	0.125	Onyx™
Job 21	D	Rectangular	Solid	1	0.125	Nylon - EoL™
Job 22	D	Rectangular	Solid	1	0.100	Nylon - EoL™

Table 1. Set of tests performed for the unreinforced components.

Fibre orientation	CF-reinforced	K-reinforced
	Test	Test
0°	Job 23	Job 29
15°	Job 24	Job 30
30°	Job 25	Job 31
45°	Job 26	Job 32
60°	Job 27	Job 33
90°	Job 28	Job 34
Process parameters (Jobs 23 to 34)	Matrix material (Nylon - EoL™): Fill pattern = Solid; Fill density = Solid; Number of section perimeters = 1; Layer thickness = According to the type of fibre.	
	Reinforced layer: Fill pattern = Isotropic; Fill density = Solid; Number of section perimeters = 1; Layer thickness = 0.125 mm (CF) or 0.100 mm (K).	

Table 2. Set of tests performed for the single-layer fibre-reinforced components ('D' geometry).

Geometries 'A' and 'B' were considered to quantify the electrical energy demand during the deposition of the Nylon - EoL™ or Onyx™ material. The two different geometries impose different deposition paths [46], and this allows the effect of the complexity (in terms of the number of turning points of the path [22]) to be analysed. Geometry 'A' was also chosen to analyse the effects of varying (*i*) the layer thickness (0.100 mm or 0.200 mm), (*ii*) the number of section perimeters (1, 2 or 4), and (*iii*) the fill pattern ('rectangular' 'solid' fill versus 30%-density 'hexagonal' fill). Geometry 'B' has a simpler geometry and was printed with a combination of a 'rectangular' fill pattern and a 'solid' fill density. Type I and Type II tensile specimens (labelled 'C' and 'D'), which were designed in accordance with ASTM D638, were produced to evaluate the effects of (*i*) the fill pattern/density, and (*ii*) the orientation of the reinforcing fibre on the energy demand. Geometry 'C' was printed in Onyx™ using the three available fill patterns (namely 'triangular', 'hexagonal', and 'rectangular'). The fill density was also varied from 'solid' to 30%. The layer thickness and the section perimeter number were set to 0.125 mm and 2, respectively. Geometry 'D' was designed to quantify the effect of the deposition of the reinforcing filament under different orientation angles. A single reinforced layer was added to the central plane (in the Z-direction) of the tensile specimen. The decision to deposit a single reinforced layer was driven by the necessity of accurately identifying the discrete stages of the deposition process (see Section 4) in order to model each energy contribution separately (see Section 5). The fill density was set as a 'solid' fill in both the matrix (made of Nylon - EoL™) and the reinforced layers. The deposition path of the reinforcing fibre was set to 'isotropic' with a single section perimeter. Six fibre deposition orientations were investigated: 0, 15, 30, 45, 60 or 90 degrees (Table 2). Figure 4 shows the deposition path in the reinforced layer for the different orientations. It can be observed that the number of turning points varies significantly according to the deposition path of the reinforcing fibre filament.

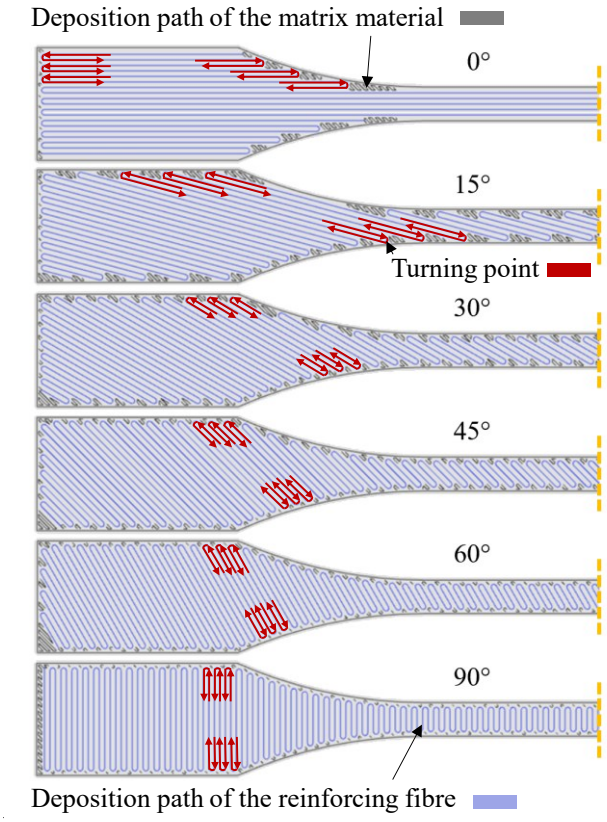

Figure 4. Deposition path of the reinforced layer for different fibre orientations (see also Table 2).

Overall, considering the whole experimental plan, the theoretical values of the average deposition rate, calculated as the ratio between the estimated print volume and the estimated print time, both of which were provided by the Eiger™ software, varied from $0.34 \cdot 10^{-1}$ cm^3/min to $2.10 \cdot 10^{-1}$ cm^3/min, which represents a satisfactory range to characterise the operating conditions of the CFF process. It is worth noting that, during the experimental tests and for the modelling purposes, the actual DR_a was obtained by quantifying the effective printing time and mass.

3.2. Energy demand assessment

The CFF machine operated as an AC single-phase system, and the electrical energy demand was measured using a Fluke 435 Series II analyser. The current, voltage, power and power factor were acquired at a high frequency and then aggregated in the analyser, which gave the results at a frequency of 4 Hz. The analyser was equipped with AC current clamps (Fluke i400s model) for the single AC phase and the neutral phase, as well as voltage clamps connected to the electricity supply wires attached to the machine. The earth reference voltage clamp was connected to the neutral phase. A power factor of approximately 0.98 was obtained for all the measurements. The electrical energy data acquisition and analysis were performed using Fluke Power Log 430-II proprietary software, Version 5.6.

3.3. Measured outcomes and modelled variables

The black-box approach to modelling the Specific Energy Consumption (*SEC*), which is well established in the literature, was applied. A correlation between the average deposition rate (DR_a) and the Specific Printing Energy (*SPE*) has already been highlighted for FDM processes [22]. DR_a quantifies the mass printed per unit time, while *SPE* represents the *SEC* evaluated only at the printing phase and is a measure of the energy required to deposit one unit of mass of material. However, as demonstrated in Sections 4 and 5, this approach requires a specific adaptation for CFF, and all the process contributions have therefore been considered separately in this research. The mass printed for each job (m_{Job}) was distinguished between (*i*) the mass of the polymer matrix content, m_{Matrix}, and (*ii*) the mass of the reinforcing fibre, i.e., CF (m_{CF}) and K (m_K), if present. The mass of the material purged to prime the extruder (m_{Purged}) was also quantified. The same approach was used for all the variables related to the energy consumption measurements. Therefore, the actual average deposition rate ($DR_{a,i}$) and the Specific Printing Energy (SPE_i) were calculated according to Eq. 1 and Eq. 2,

$$DR_{a,i} = \frac{m_i}{t_i} \quad (1)$$

$$SPE_i = \frac{E_i}{m_i} \quad (2)$$

where *i* indicates the different materials (*i* = 'Matrix', or 'CF', or 'K').

After the production, each part was weighed using a Gibertini 1000HR-CM balance with a resolution of 0.01 g. Because of the complexity of performing a direct measurement, the mass of the reinforced layer (m_{CF} or m_K) of the reinforced components was determined from the printed volume, as provided by the Eiger™ software, and using the nominal density (Table 3) given in the material data sheet [45]. The mass of the matrix in the reinforced components (m_{Matrix}) was then obtained as the difference between the mass of the component and that of the fibre (m_{CF} or m_K). The time (t_{Matrix}, t_{CF} and t_K) and electrical energy requirements (E_{Matrix}, E_{CF} and E_K) for the printing phase were extracted from the power profile over the manufacturing time. The different process steps were identified, as detailed in Section 4, while the energy consumption model is presented in Section 5.

Material	Nylon - EoL™	Onyx™	CF	K
Density [g/cm^3]	1.1	1.2	1.4	1.2

Table 3. Material properties taken from the Markforged® data sheets [45].

4. Experimental results

According to the process description in Section 2, the different phases of the process were identified, as detailed in Section 4.1, and all the energy requirements are summarised in Section 4.2 as a function of the deposition time and deposited mass.

4.1. Process characterisation

The electrical energy variables (e.g., current and power profiles) were recorded as a function of the process time. These profiles were found to be similar for all the tested conditions, with slight variations that depended on the number of layers and the presence - or not - of reinforced layers, and they allowed the main phases of the CFF process to be highlighted: (1) start-up (powering of the machine), (2) process setup (which includes loading the Job file and glueing the build plate, i.e., the activities the operator is in charge of), (3) machine warm-up (which includes extruder heating and calibration of the axes), (4) the actual printing phase, and (5) shutdown (which includes removing the 3D printed component and any residual glue from the build plate).

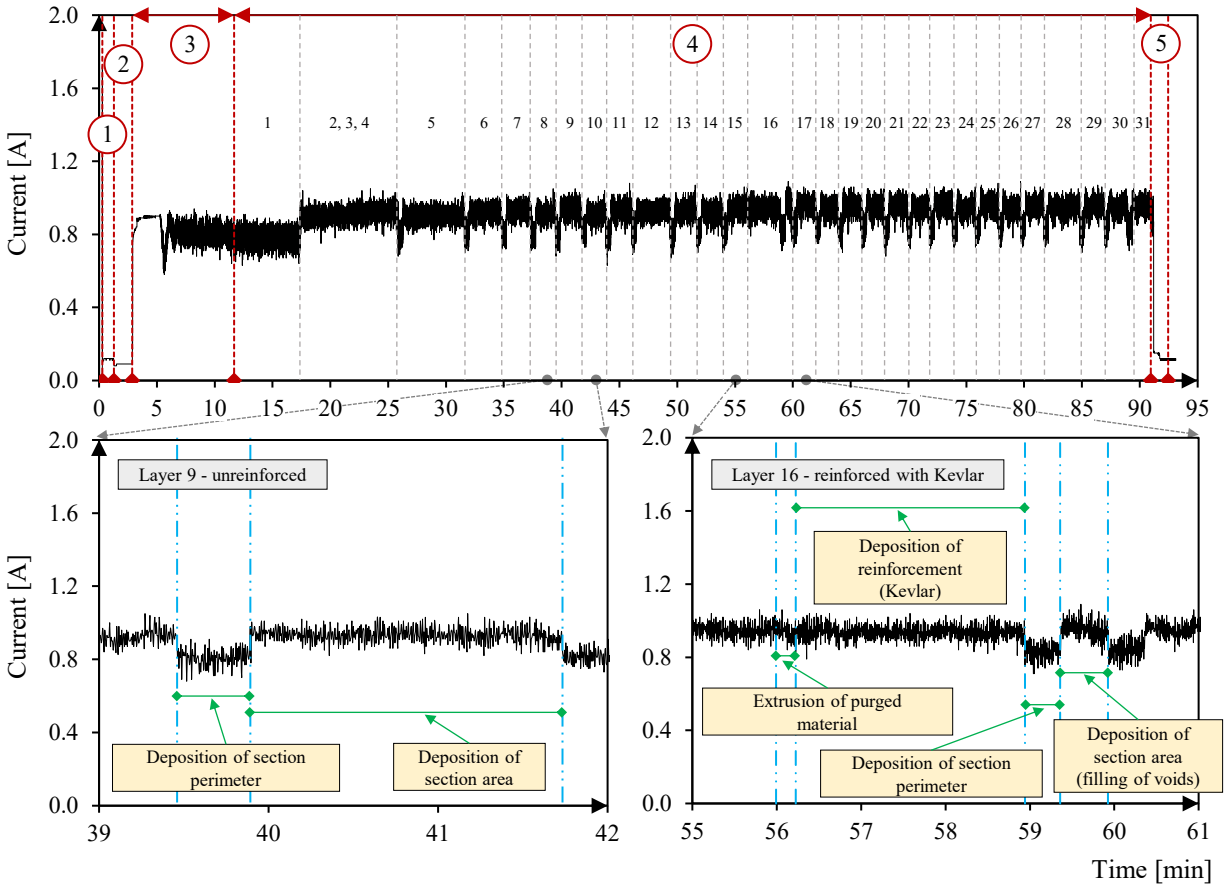

Figure 5. An example of current profile acquisition, referring to Job 30.
Process phases from (1) to (5) are labelled as explained in Section 4.1.

Figure 5 plots the current profile of the MarkTwo™ machine during the production of Job 30 (see Table 2). There are 31 printed layers, and the central layer (layer #16) is reinforced with Kevlar. The start and end of the deposition of each layer can be distinguished from the drop in the current demand, and they are highlighted in

Figure 5 with dashed lines. The printing of the component begins with the deposition of the matrix layers. Moreover, a small amount of matrix material is purged for each reinforced layer before starting the deposition of the next layer. Overall, the deposition time of each layer is quite constant, except for the first layers and the reinforced one. The deposition speed is lower for the first layers to ensure a better adherence of the printed component to the build plate. The deposition speed appears to be higher from the fifth layer onwards. The speed for the reinforced layer is slower than that for the full matrix layer. This result is particularly evident for the selected reinforced components, because the geometry has a constant cross section along the build direction. The lower deposition speed for the reinforcing fibre filament is necessary to ensure a good adhesion of the fibre filament with the preceding matrix layer and between two fibre tracks, thereby reducing the risk of filament breakage at the turning point. For the reinforced layer, the average duration of the purged material deposition is 14 seconds and the layer is completed by depositing the Nylon - EoL^{TM} matrix along the section perimeter and into the voids of the inner area. After the deposition of the reinforced layer, each unreinforced layer undergoes a rapid alternation of its section perimeter and inner area, as the purged material is no longer required.

4.2. Electrical energy demand

Process phases (1), (2), and (5) are independent of the process conditions. Phase (3), i.e., the machine warm-up, is affected by the type of material being printed. Table 4 summarises the average time and energy demand values of all the jobs for process phases (1), (2), (5), and (3) as functions of the printed material. The deviation of the experimental data from the average value was found to be less than 5%.

Process phase		Time [min]		Energy demand [Wh]	
(1) Start-up		t_1	1.0	E_1	< 0.1 *
(2) Process setup		t_2	1.5	E_2	0.3
(3) Machine warm-up	Unreinforced Nylon - EoL^{TM} components	t_3	8.4	E_3	13.5
	Unreinforced Onyx^{TM} components	t_3	8.4	E_3	14.0
	Fibre-reinforced components	t_3	8.6	E_3	14.2
(5) Shutdown		t_5	1.5	E_5	0.3

Table 4. Time and electrical energy demand for phases (1), (2), (3) and (5). The value marked with * was calculated as 0.01 Wh.

The measurement results for the phase (4), in terms of printed mass, printing time and printing energy, are given in Figure 6 for the unreinforced components (Table 1), and in Figure 7 and Table 5 for the fibre-reinforced components (Table 2), where the contribution of each material deposition is highlighted according to Section 4.1. Table 5 shows that the time and energy results (t_{Matrix} and E_{Matrix}) pertaining to the matrix material deposited with the two reinforcement fibres differ. However, this difference is only due to the different layer thicknesses that are automatically selected once the fibre type has been set (see also Table 2). On the other hand, the time (i.e., either t_{CF} or t_K) and energy (E_{CF} or E_K) required for the fibre deposition varies according to the orientation of the fibres, which is directly influenced by the number of turning points in the deposition

path (see Figure 3). The multiple accelerations and decelerations of the deposition head at the turning points slow down the overall deposition speed to a great extent. Based on these findings, the use of energy-intensive fibre orientations, such as 90°, should be limited to critical regions where they are essential, such as in areas that require multi-directional bending resistance. In real-world manufacturing, where the components often experience complex loading conditions, such components may incorporate multiple fibre orientations to achieve both optimal structural performance and energy-efficient production. The average deposition rate (DR_a) values experimentally calculated according to Eq. 1 range from $3.07 \cdot 10^{-3}$ kg/h to $1.37 \cdot 10^{-2}$ kg/h for the geometries printed with the matrix material, and from $3.44 \cdot 10^{-3}$ kg/h to $6.63 \cdot 10^{-3}$ kg/h for only the deposition of the reinforcing fibre, as detailed in the Appendix. Despite the differences in the values calculated using the software estimates, the variation in DR_a has been confirmed to be representative of the typical operating conditions of the CFF process.

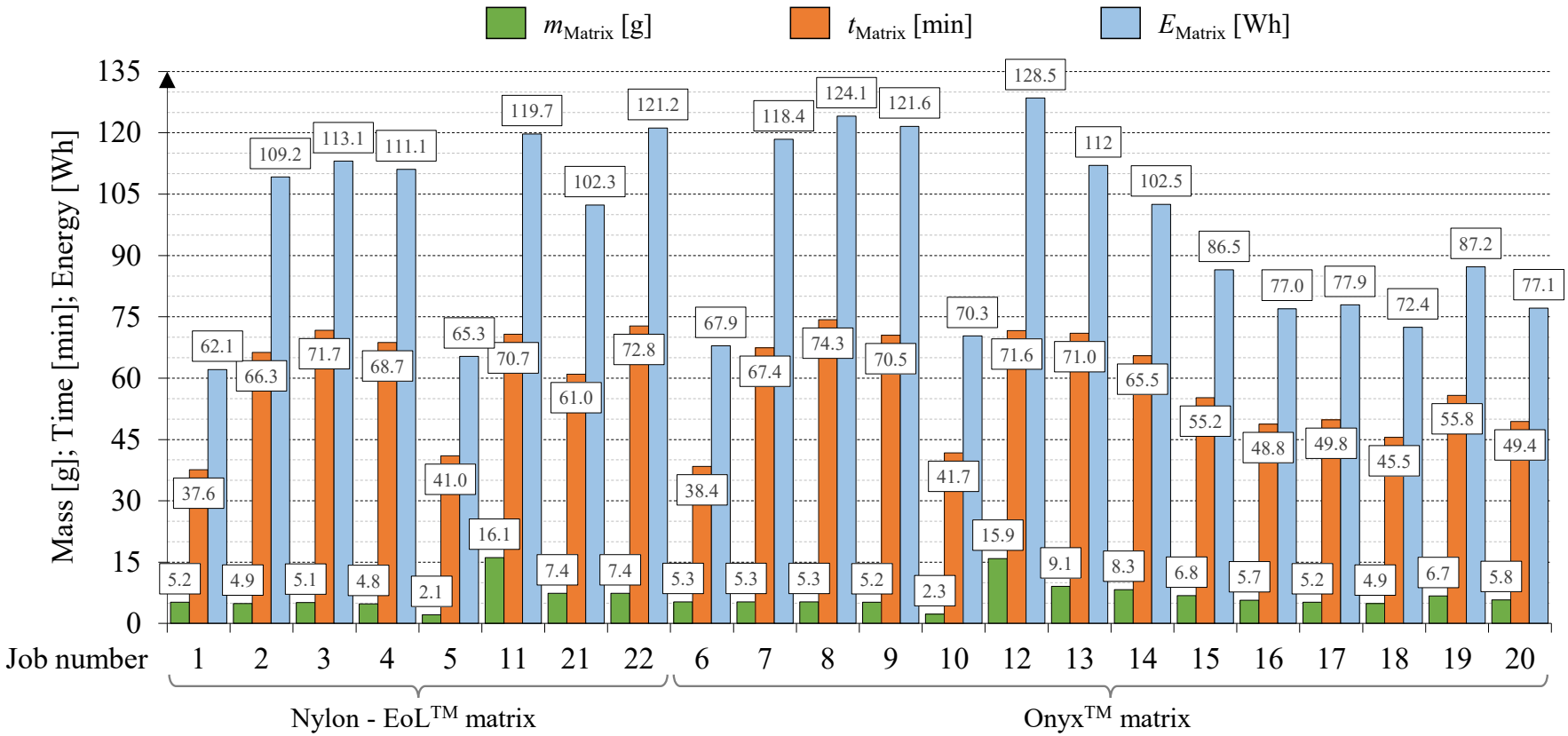

Figure 6. Printing phase (4) of the unreinforced components: mass, time and energy results.

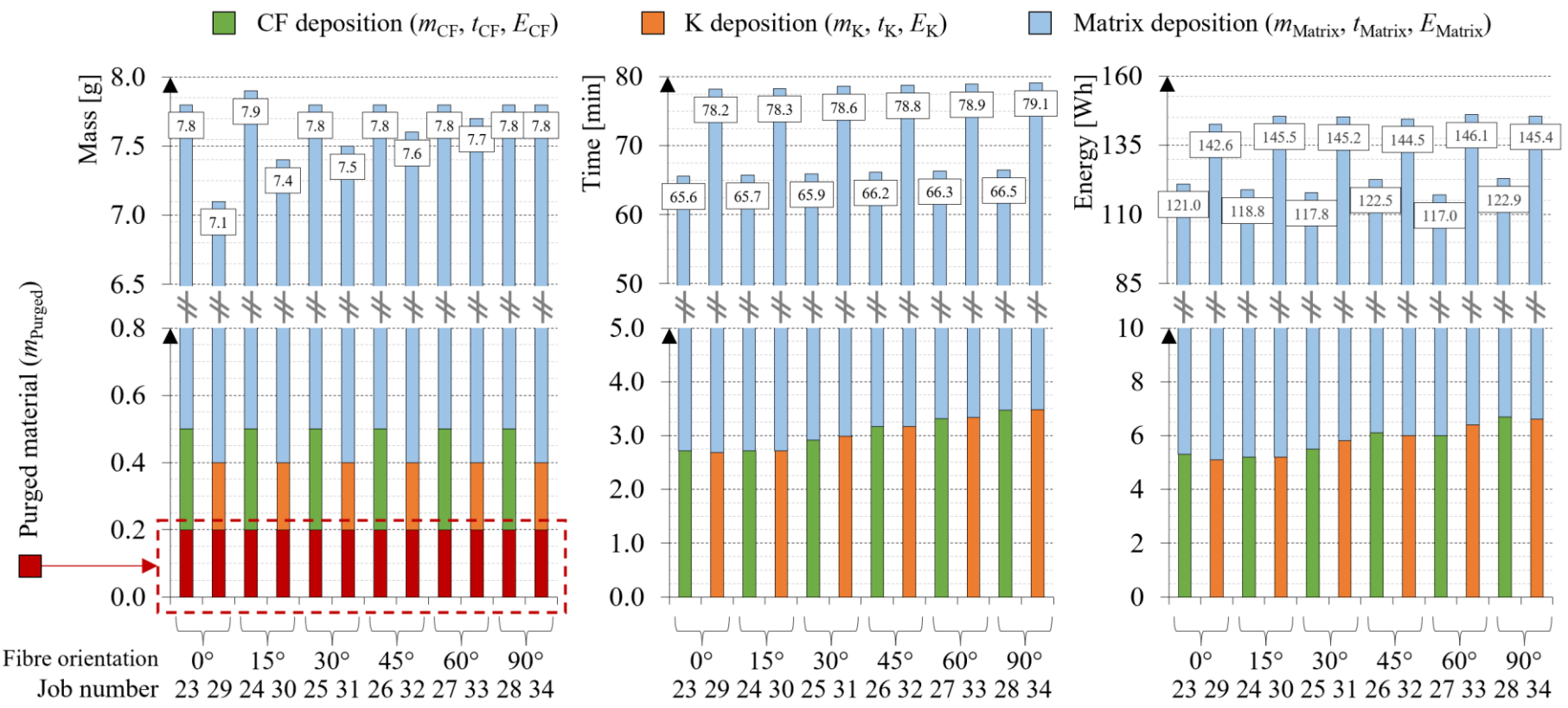

Figure 7. Printing phase (4) of the reinforced components: mass, time and energy results. Only a single layer was either CF- or K-reinforced (i.e., for Job 23 to 34, according to Table 2).

Fibre orientation	CF-reinforced							K-reinforced						
	Test	m_{Matrix} [g]	m_{CF} [g]	t_{Matrix} [min]	t_{CF} [min]	E_{Matrix} [Wh]	E_{CF} [Wh]	Test	m_{Matrix} [g]	m_{K} [g]	t_{Matrix} [min]	t_{K} [min]	E_{Matrix} [Wh]	E_{K} [Wh]
0°	Job 23	7.3	0.3	62.9	2.7	115.7	5.3	Job 29	6.7	0.2	75.5	2.7	137.5	5.1
15°	Job 24	7.4	0.3	63.0	2.7	113.6	5.2	Job 30	7.0	0.2	75.6	2.7	140.3	5.2
30°	Job 25	7.3	0.3	63.0	2.9	112.3	5.5	Job 31	7.1	0.2	75.6	3.0	139.4	5.8
45°	Job 26	7.3	0.3	63.0	3.2	116.4	6.1	Job 32	7.2	0.2	75.6	3.2	138.5	6.0
60°	Job 27	7.3	0.3	63.0	3.3	111.0	6.0	Job 33	7.3	0.2	75.6	3.3	139.7	6.4
90°	Job 28	7.3	0.3	63.0	3.5	116.2	6.7	Job 34	7.4	0.2	75.6	3.5	138.8	6.6

Table 5. Printing phase (4) of the reinforced components: mass, time and energy demand. The mass of purged material (m_{Purged}) was 0.2g in all the tests. The values are rounded off to the first decimal place.

5. Modelling of the energy consumption

This section is divided into four parts. Section 5.1 discusses the relationship between the printing energy, printing time and printed mass. Section 5.2 details the approach proposed here to quantify the specific printing energy necessary for the deposition of either the matrix or reinforcing materials. The model used to estimate the total energy consumption of the CFF process is presented in Section 5.3 and validated in Section 5.4.

5.1. Printing energy, printing time and printed mass

The total energy demand of the printing phase (E_4) is plotted in Figure 8 as a function of the printing time (t_4) and the total mass printed (m_{Job}) for all the experimental tests. As can be observed, the relationship between E_4 and t_4 within the selected range of process parameters can be approximated by a linear regression model (Figure 8*a*). The higher the printing time is, the higher the printing energy. This result is consistent with previous findings in the literature on AM processes in which polymer filaments [22, 47], metal wire [48] and metal powders [17, 49-51] were used. On the other hand, there appears to be no correlation between E_4 and m_{job} (Figure 8*b*). These results are related to the trend of the power demand during deposition, which is almost constant over time (see also Figure 5), with only slight deviations from the average value due to the different features being deposited in both the reinforced and unreinforced layers. The time-dependency of the energy requirement confirms the choice of considering the deposition rate (which relates the amount of mass deposited to the unit of time, which in turn is related to the complexity of the specific features and the deposition path) when modelling the specific energy consumption, rather than the mass deposited alone.

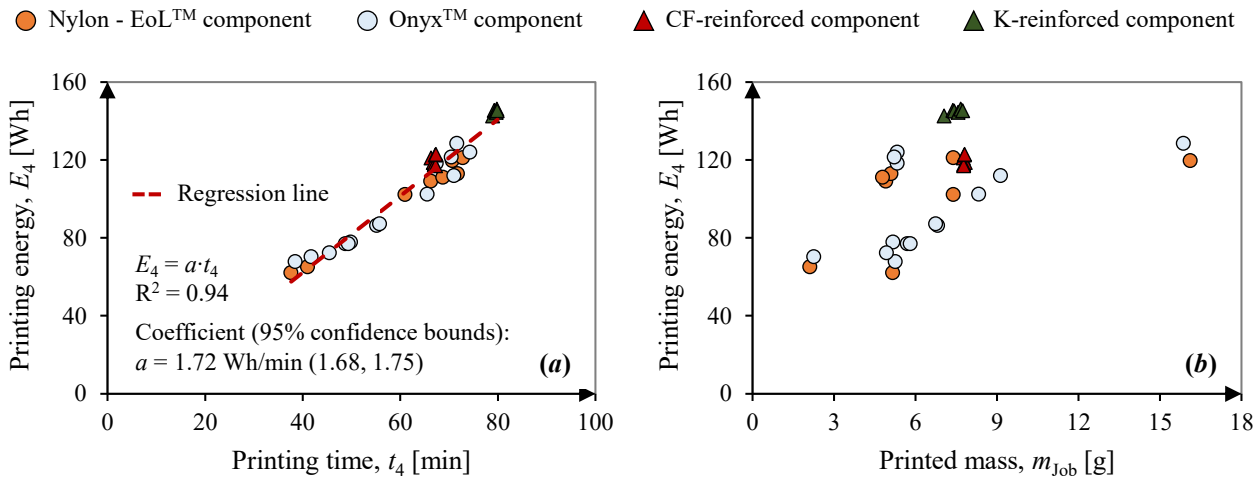

Figure 8. Printing phase (4): experimental correlation between the printing energy and printing time (*a*) or printed mass (*b*).

Looking at the reinforced layer only, Figure 9 shows that the higher the angle of fibre deposition is (i.e., from 0° to 90°), the longer the time. This result is related to the number of turning points (Figure 3). The multiple acceleration and deceleration ramps, due to the turning points, significantly reduce the overall deposition speed. The time necessary to deposit the external perimeter ($t_{contour}$) is approximately 0.5 min for all the printed components, as the outer path is always the same. However, the time spent filling the remaining voids, after

the deposition of the reinforcing fibre (t_{gap}), depends on the deposition path. Indeed, t_{gap} increases for the reinforcing fibres when the orientation angle increases from 0° to 15°, and then decreases slightly. The time needed to deposit the CF and K fibres is similar (Figure 9*a*). The total printing time of the CF- and K-reinforced components mainly differs because the Nylon-EoL^{TM} matrix is deposited with two different layer thicknesses. Similar considerations apply for the energy required to deposit the reinforcing fibre (E_{CF}, E_K), for the contour ($E_{contour}$), and to fill the gaps (E_{gap}).

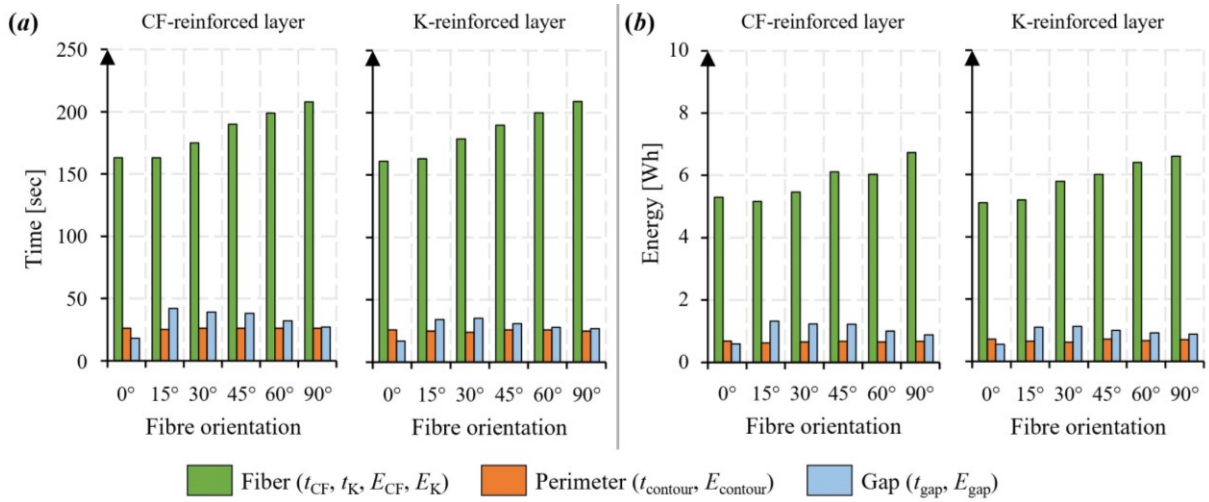

Figure 9. Time (*a*) and energy demand (*b*) necessary to deposit the reinforced layer (Geometry: 'D').

5.2. Specific printing energy

Considering the results presented above, the *SPE* has been plotted as a function of DR_a [17, 22] in Figure 10, where the deposition values of the reinforced layers are clustered separately from those of the unreinforced components. This visual representation suggests that the CFF process has a different performance in the deposition of the matrix and of the reinforcing filament. All the values related to the matrix materials (i.e., from Job 1 to Job 22) can be approximated by the same regression curve. The results of Job 5 and Job 10 demonstrate that using an infill pattern and density that require a more complex path could lead to a lower deposition rate and higher specific printing energy. The simplest deposition path, when combined with thicker layers, significantly reduces the specific printing energy (e.g., in Jobs 11 and 12). The printing of Onyx^{TM} requires a slightly higher average power demand than that of Nylon-EoL^{TM}, which could be explained by the higher required temperature. As far as the reinforced layers of Jobs 23 to 34 are concerned, once the fibre orientation and the layer geometry have been set, the Markforged® Eiger^{TM} software generates a unique deposition path that is independent of the reinforcing fibre filament. The values of the CF- and K-reinforced layers are on the same regression curve, despite the variation in reinforcing fibre and fibre orientation. Given that the deposition path remains constant, the discrepancy in specific printing energy can be attributed to the variation in the density of the reinforcement materials, which affects the estimated deposited masses. Moreover, a higher fibre orientation (from 0° to 90°) increases the deposition time, due to the more complex path, which has more acceleration and deceleration ramps (Figure 4). The SPE_{Matrix} and $DR_{a,\,Matrix}$ values of the reinforced components show only a slight variation from those of the unreinforced components, due to the

similar process and part designs of the matrices. It should be noted that these outcomes could drive the choice of structural reinforcement material and design prior to the manufacturing phase, if the different performances of the reinforcements with varying fibre types are taken into account.

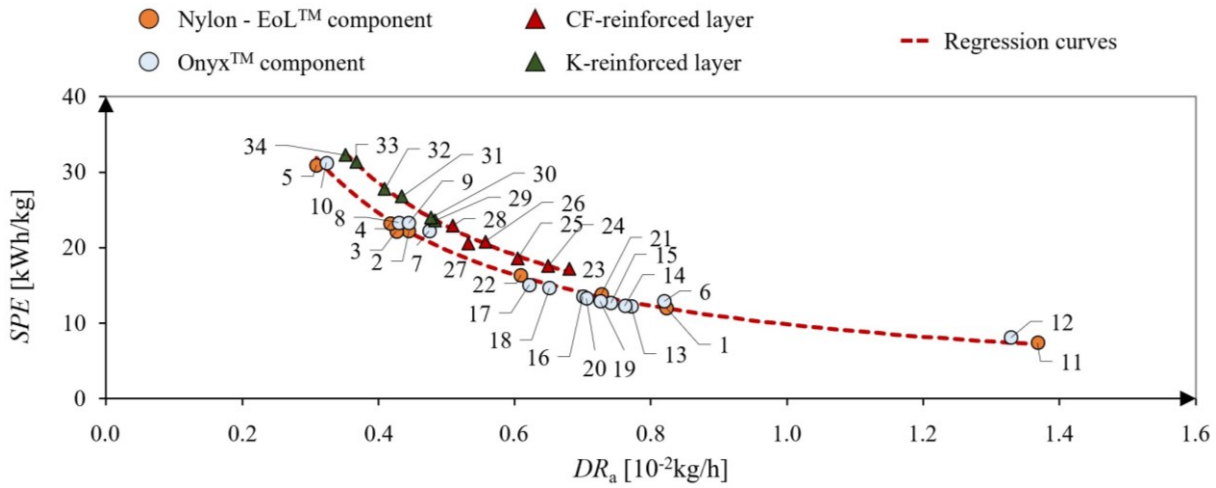

Figure 10. Correlation between *SPE* and DR_a. Full part deposition was considered for the unreinforced components, while the values corresponding to the reinforced layer deposition are shown for the reinforced components.

Given the hyperbolic regression curves of each subset of materials, the constant C_i (in kWh/h) that correlates the *SPE* and DR_a can be calculated. The values of C_i with 95% confidence limits and the corresponding R^2 value of the reinforced layers and matrix materials are given in Table 6.

Parameter	C_i [kWh/h]	95% confidence bounds [kWh/h]	R^2
C_{Matrix}	$9.84 \cdot 10^{-2}$	$(9.67 \cdot 10^{-2}, 10.01 \cdot 10^{-2})$	0.99
$C_{CF} = C_K$	$11.43 \cdot 10^{-2}$	$(11.31 \cdot 10^{-2}, 11.56 \cdot 10^{-2})$	0.99

Table 6. Values of the regression constant C_i of the model (i.e., C_{Matrix}, C_{CF} or C_K).

Therefore, SPE_{Matrix} and SPE_{CF}, or SPE_K, can be modelled according to Eq. 3 and Eq.4, respectively,

$$SPE_{\text{Matrix}} = \frac{C_{\text{Matrix}}}{DR_{\text{a,Matrix}}} = \frac{9.84 \cdot 10^{-2}}{DR_{\text{a,Matrix}}} \quad (3)$$

$$SPE_{\text{CF (or K)}} = \frac{C_{\text{CF (or K)}}}{DR_{\text{a,CF (or K)}}} = \frac{11.43 \cdot 10^{-2}}{DR_{\text{a,CF (or K)}}} \quad (4)$$

where:

- SPE_i: specific energy demand (in kWh/kg) of only the printing phase (i.e., SPE_{Matrix}, SPE_{CF} or SPE_K);
- $DR_{a,\,i}$: average deposition rate (in kg/h) of the printing phase (i.e., $DR_{a,\,Matrix}$; $DR_{a,\,CF}$ or $DR_{a,\,K}$).

5.3. Energy requirements for CFF

From the results of Section 5.2, it can be seen that the total specific printing energy necessary to produce a reinforced component (SPE_{Job}) can be obtained by combining the *SPE* contributions related to the matrix deposition and the one related to the deposition of the reinforcing material. The proposed model is presented in Eq. 5.

$$SPE_{\mathrm{Job}} = \frac{E_4}{m_{\mathrm{Job}}} = \frac{E_{\mathrm{CF\ (or\ K)}} + E_{\mathrm{Matrix}}}{m_{\mathrm{Job}}} = \frac{E_{\mathrm{CF\ (or\ K)}}}{m_{\mathrm{CF\ (or\ K)}}} \cdot \frac{m_{\mathrm{CF\ (or\ K)}}}{m_{\mathrm{Job}}} + \frac{E_{\mathrm{Matrix}}}{m_{\mathrm{Matrix}}} \cdot \frac{m_{\mathrm{Matrix}}}{m_{\mathrm{Job}}} =$$

$$= SPE_{\mathrm{CF\ (or\ K)}} \cdot \frac{m_{\mathrm{CF\ (or\ K)}}}{m_{\mathrm{Job}}} + SPE_{\mathrm{Matrix}} \cdot \frac{m_{\mathrm{Matrix}}}{m_{\mathrm{Job}}} = \frac{C_{\mathrm{CF\ (or\ K)}}}{DR_{\mathrm{a,CF\ (or\ K)}}} \cdot \frac{m_{\mathrm{CF\ (or\ K)}}}{m_{\mathrm{Job}}} + \frac{C_{\mathrm{Matrix}}}{DR_{\mathrm{a,Matrix}}} \cdot \frac{m_{\mathrm{Matrix}}}{m_{\mathrm{Job}}} \quad (5)$$

Taking into account the experimental values obtained in this research (i.e., Eq. 3 and Eq.4), Eq. 5 can be rewritten as Eq. 6.

$$SPE_{\mathrm{Job}} = \frac{11.43 \cdot 10^{-2}}{DR_{\mathrm{a,CF\ (or\ K)}}} \cdot \frac{m_{\mathrm{CF\ (or\ K)}}}{m_{\mathrm{Job}}} + \frac{9.84 \cdot 10^{-2}}{DR_{\mathrm{a,Matrix}}} \cdot \frac{m_{\mathrm{Matrix}}}{m_{\mathrm{Job}}} \quad (6)$$

As a result, the printing energy, E_4, can be assessed using Eq. 7, as a function of the total printed mass (m_{job}).

$$E_4 = m_{\mathrm{Job}} \cdot SPE_{\mathrm{Job}} \quad (7)$$

Table 7 shows a comparison of the experimental and calculated E_4 values obtained using Eq. 7 for all the reinforced components. As can be observed, the calculated values deviate from the experimental values by an average negative relative error of about 8.5%. Therefore, E_4 is underestimated for the reinforced components, with respect to the experimental value. This difference could be partially explained by considering the contribution of the purged material present during the printing of the reinforced components, which was not included in the regression model. Therefore, Eq. 7 could be corrected for reinforced components as shown in Eq. 8,

$$E_4 = m_{\mathrm{Job}} \cdot SPE_{\mathrm{Job}} + n \cdot e_{\mathrm{pur}} \quad (8)$$

where e_{pur} is the specific energy (quantified as 0.42 Wh/layer) required to purge the material before each layer is printed, and n is the total number of layers up to the last reinforced layer. The values of E_4 calculated according to Eq. 8 (Table 7) compensate for a part of the error, which is reduced to about 5%. The remaining deviation appears to be small and within the confidence interval. Considering the contributions of all the process phases (Table 4), the total energy demand (E_{CFF}) and the *SEC* of the whole process can be quantified by Eq. 9 and Eq. 10, respectively.

$$E_{\mathrm{CFF}} = E_1 + E_2 + E_3 + E_4 + E_5 \quad (9)$$

$$SEC = \frac{E_{\mathrm{CFF}}}{m_{\mathrm{Job}}} \quad (10)$$

Test	m_{Job} [g]	E_4 [Wh], measured	SPE_{Job} [kWh/kg], according to Eq. 6	E_4 [Wh], according to Eq. 7	Error [%], applying Eq. 7	n	E_4 [Wh], according to Eq. 8	Error [%], applying Eq. 8
Job 23	7.8	121.0	14.1	109.5	-9.5	13	114.9	-5.0
Job 24	7.9	118.8	14.1	110.2	-7.2	13	115.7	-2.6
Job 25	7.8	117.7	14.3	110.6	-6.0	13	116.1	-1.4
Job 26	7.8	122.5	14.2	111.0	-9.4	13	116.5	-5.0
Job 27	7.8	117.0	14.3	111.1	-5.1	13	116.6	-0.4
Job 28	7.8	122.9	14.3	111.3	-9.5	13	116.7	-5.0
Job 29	7.1	142.6	18.5	130.1	-8.8	16	136.8	-4.0
Job 30	7.4	145.4	17.7	130.7	-10.1	16	137.4	-5.5
Job 31	7.5	145.2	17.7	131.2	-9.6	16	137.9	-5.0
Job 32	7.6	144.5	17.4	131.5	-9.0	16	138.2	-4.4
Job 33	7.7	146.1	17.2	131.8	-9.8	16	138.5	-5.2
Job 34	7.8	145.4	17.1	131.9	-9.3	16	138.6	-4.6

Table 7. Printing energy, E_4: comparison of the experimental and modelled values. The calculations were made using all the significant digits and the results are rounded off to the first decimal place.

5.4. Validation of the model

A new part was considered for validation purposes. The geometry is a cover (shown in Figure 11*a* and labelled 'E'), which was designed to include several features that could characterise a typical composite part manufactured using CFF (e.g., thin walls, large cross-sectional variations, holes and multiple reinforced layers). The base of the cover has a maximum envelope of 72 mm × 48 mm × 17 mm (height). The cover is 2 mm thick. The cover was produced with four layers reinforced with carbon fibre and with different orientations (Job 35). The layers were numbered in ascending order from the build plate, with layer 5 and layer 12 being reinforced with the fibre deposited at 0° (Figure 11*b*), and layer 6 and layer 11 being reinforced with a fibre orientation of 90° (Figure 11*c*). The matrix material was applied with '4 section perimeters'. The fill pattern was set to 'solid' fill in both the matrix and reinforced layers. The cover was also made entirely of Nylon - EoL^{TM} (Job 36) for benchmarking purposes, with (*i*) a layer thickness of 0.100 mm, (*ii*) 4 perimeters, and (*iii*) a 62%-density 'hexagonal' fill pattern.

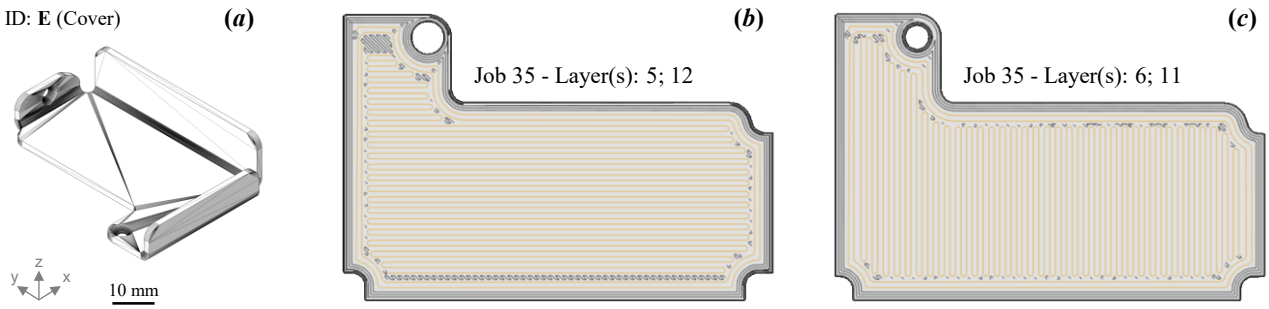

Figure 11. Geometry adopted for the validation tests (*a*) and details of fibre orientation: 0° (*b*) and 90° (*c*).

The validation was performed by comparing the value of E_4 estimated using the proposed model with the experimental value (Table 8). The estimated E_4 was calculated from Eq. 7, where SPE_{Job} was quantified using Eq. 6. Each reinforced layer weighed approximately 0.3 g, which led to a total of 1.2 g for the four layers. The deposition of each reinforced layer with the 0° orientation lasted 171.5 s, while it lasted 179.0 s for the 90° orientation, due to the higher number of turning points (see Figures 11*b* and 11*c*). Therefore, the total printing time of the reinforced layers was 701 s. The energy requirement for each reinforced layer of the 0° and 90° fibre orientations was 5.6 Wh and 5.8 Wh, respectively. Overall, the comparison between the E_4 values showed a satisfactory capacity of the model to estimate the printing energy demand, with a deviation between the experimental and the estimated values of less than 3%, that is, within the confidence interval. The new data are also positioned on the *SPE* versus DR_a curves determined empirically according to Eq. 3 and Eq. 4, thus confirming the proposed approach (Figure 12).

Test	t_{Matrix} [min]	t_{CF} [sec]	m_{Matrix} [g]	m_{CF} [g]	E_{Matrix} [Wh]	E_{CF} [Wh]	SPE_{Job} [kWh/kg]	E_4 [Wh]	SPE_{Job} [kWh/kg], according to Eq. 6	E_4 [Wh], according to Eq. 7
Job 35	82.2	701.0	7.3	1.2	138.5	22.8	19.0	161.3	18.5	157.1
Job 36	108.7	-	7.3	-	176.3	-	24.2	176.3	24.4	178.3

Table 8. Results of the model validation. The calculations were made using all the significant digits and the results are rounded off to the first decimal place.

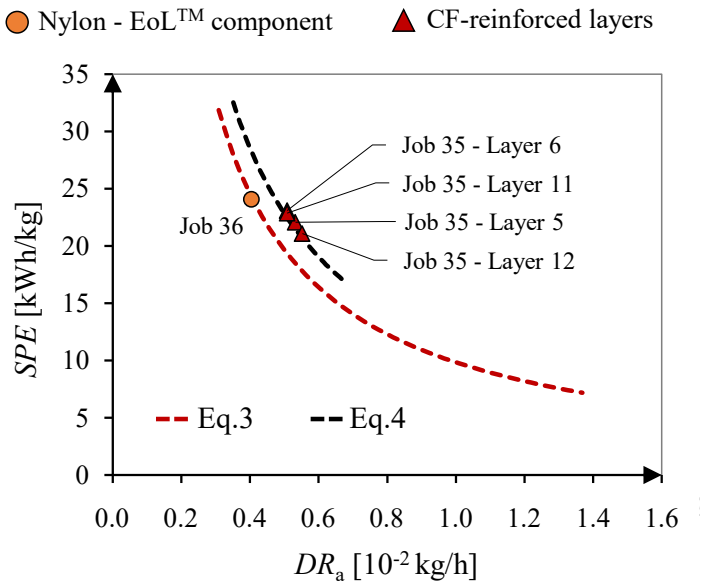

Figure 12. Positioning of Job 35 and each reinforced layer for Job 36 on the *SPE* vs. DR_a curves from Eq. 3 and Eq. 4.

6. Conclusions and outlooks

The data pool available on the energy required to produce composite parts, although scattered, is growing. However, there is a large gap in knowledge pertaining to additive manufacturing technologies. A model for the energy demand of the Continuous Fibre Fabrication (CFF) process has been presented in this work. The process was studied by varying several deposition conditions, such as the process parameters, part geometries, and reinforcing fibre and matrix materials, while characterising the energy demand as a function of the deposition rate. Overall,

- the DR_a values for CFF appeared to be significantly lower than those of the other FDM systems (0.6-6.0·10^{-2} kg/h, according to [22]);
- *SEC* values ranging from 161 to 218 MJ oil-equivalent (i.e., from 17 to 23 kWh/kg, assuming a primary-to-secondary energy conversion efficiency of 0.38 [34]) were obtained for the production of the fibre-reinforced components.

The obtained results confirm the possibility of assuming *SEC* as a holistic parameter to describe the variation in the energy demand as a function of the key manufacturing process variables (the average deposition rate in the case of additive manufacturing), as already discussed in Section 1. Nonetheless, a specific adaptation is required for CFF, since the process operates under two regimes: one for the deposition of the matrix material and one for the deposition of the reinforcing fibre material, where a lower speed is required for the latter to guarantee a good adhesion with the previous layer and between two adjacent tracks. Although the theoretical conceptualisation of the model, which is based on the separation of *SEC* contributions related to the deposition of either matrix or reinforcement materials, is realistically generalisable, some limitations should be pointed out. First, the obtained results are specific of the CFF process/test conditions that were investigated (equipment, components, materials and process parameters) and are difficult to extend to other combinations of FRPs and MEX/FDM processes. Second, the research can be further refined to include other variables, such as equipment wear and/or other external factors. The observed sources of uncertainty and errors are related to the input data, which refer to small-to-medium-sized components and low energy/material requirements, and this may be reflected in the scale-up calculation of the *SEC* values in kWh/kg and MJ/kg, which is, however, necessary to compare CFF with other production routes. Finally, the analysis was limited to a single unit process, which needs to be contextualised within the life cycle of the product to fully understand the environmental sustainability implications, as the higher energy requirements of AM could be offset by a lower raw material consumption.

Although the *SEC* values achieved in this research appear to be higher than those of conventional high-productivity manufacturing routes, they may be lower than or comparable to those of low-volume processes, where AM has already been shown to be competitive and effective, but offer shorter lead times and lower costs. Therefore, CFF may be a potential sustainable alternative for industries involved in manufacturing complex composite components, where the number of parts produced is small or made-to-order, and where the benefits may also be related to avoiding moulds or tooling. Moreover, improvements in energy efficiency could also be achieved through technological advances, including machine, process/product optimisation and

material innovations. According to the obtained results, the time-dependency of the energy demand could benefit from any increase in printing speed. Material innovation could lead to lower extrusion temperatures or improved viscosity for faster and more efficient printing. Changes in process and product design could be introduced to adjust the placement of the fibres to ensure deposition only where needed, thereby reducing energy during the most energy-intensive phases. Optimisation of the model could be achieved, while taking into account the main factors that influence *SEC* (i.e., the presence of the reinforcing fibre and the fibre orientation or the matrix infill, ergo the number of turning points), by considering the process and the part design simultaneously. Choosing a fibre orientation that reduces the number of turning points, while still meeting the mechanical requirements, improving the fibre distribution by limiting the number of reinforcing layers or only localising the reinforced fibre, could all reduce the energy requirements of the process. Apart from the mechanical properties, material sustainability is another crucial consideration in the design of composite materials, especially for the CFF process. It is well known that the sustainability of composite materials is often limited by challenges in recycling, primarily because it is difficult to separate the matrix from the fibre. However, with CFF, the rational use of reinforcing fibres only where they are strictly required not only improves energy efficiency but also increases the potential recyclability of the materials. By minimising unnecessary reinforcement, CFF enables a more efficient usage of the materials, thereby potentially reducing the environmental footprint of composite products. However, the scalability of this trade-off depends on the specific application. In scenarios where maximum performance is necessary, such as the production of aerospace or automotive safety-critical components, energy consumption at the manufacturing level may be a justifiable cost, whenever the overall product life is considered. For less demanding applications, where energy efficiency is prioritised, the selective use of fibre orientations may offer a way of optimising both energy consumption and the mechanical performance. Therefore, further studies are needed to develop indicators that consider the relationship between energy consumption and in-use performance (e.g. mechanical) to identify the best trade-off between technological performance and environmental sustainability.

Declaration of competing interest

The authors declare that they have no known competing financial interests or personal relationships that could have appeared to influence the work reported in this paper.

Appendix

Test	$DR_{a,\ Matrix}$ [kg/h]	$DR_{a,\ CF}$ or $DR_{a,\ K}$ [kg/h]
Job 1	$8.30 \cdot 10^{-3}$	-
Job 2	$4.43 \cdot 10^{-3}$	-
Job 3	$4.27 \cdot 10^{-3}$	-
Job 4	$4.19 \cdot 10^{-3}$	-
Job 5	$3.07 \cdot 10^{-3}$	-
Job 6	$8.28 \cdot 10^{-3}$	-
Job 7	$4.72 \cdot 10^{-3}$	-
Job 8	$4.28 \cdot 10^{-3}$	-
Job 9	$4.43 \cdot 10^{-3}$	-
Job 10	$3.31 \cdot 10^{-3}$	-
Job 11	$1.37 \cdot 10^{-2}$	-
Job 12	$1.33 \cdot 10^{-2}$	-
Job 13	$7.69 \cdot 10^{-3}$	-
Job 14	$7.60 \cdot 10^{-3}$	-
Job 15	$7.39 \cdot 10^{-3}$	-
Job 16	$7.01 \cdot 10^{-3}$	-
Job 17	$6.27 \cdot 10^{-3}$	-
Job 18	$6.46 \cdot 10^{-3}$	-
Job 19	$7.20 \cdot 10^{-3}$	-
Job 20	$7.04 \cdot 10^{-3}$	-
Job 21	$7.28 \cdot 10^{-3}$	-
Job 22	$6.10 \cdot 10^{-3}$	-
Job 23	$6.96 \cdot 10^{-3}$	$6.63 \cdot 10^{-3}$
Job 24	$7.05 \cdot 10^{-3}$	$6.63 \cdot 10^{-3}$
Job 25	$6.95 \cdot 10^{-3}$	$6.17 \cdot 10^{-3}$
Job 26	$6.95 \cdot 10^{-3}$	$5.68 \cdot 10^{-3}$
Job 27	$6.95 \cdot 10^{-3}$	$5.43 \cdot 10^{-3}$
Job 28	$6.95 \cdot 10^{-3}$	$5.19 \cdot 10^{-3}$
Job 29	$5.32 \cdot 10^{-3}$	$4.47 \cdot 10^{-3}$
Job 30	$5.56 \cdot 10^{-3}$	$4.42 \cdot 10^{-3}$
Job 31	$5.63 \cdot 10^{-3}$	$4.02 \cdot 10^{-3}$
Job 32	$5.71 \cdot 10^{-3}$	$3.79 \cdot 10^{-3}$
Job 33	$5.79 \cdot 10^{-3}$	$3.60 \cdot 10^{-3}$
Job 34	$5.87 \cdot 10^{-3}$	$3.44 \cdot 10^{-3}$

Table A.1. Deposition rate of all the considered test conditions and of each material.

References

[1] Herrmann C, Dewulf W, Hauschild M, Kaluza A, Kara S, Skerlos S. Life cycle engineering of lightweight structures. CIRP Ann 2018;67:651–72. https://doi.org/10.1016/j.cirp.2018.05.008.

[2] Mckinsey. Reverse the curse: Maximizing the potential of resource-driven economies 2013. https://www.mckinsey.com/industries/metals-and-mining/our-insights/reverse-the-curse-maximizing-the-potential-of-resource-driven-economies. Accessed on October 30, 2024.

[3] Steffen W, Broadgate W, Deutsch L, Gaffney O, Ludwig C. The trajectory of the Anthropocene: The Great Acceleration. Anthr Rev 2015;2:81–98. https://doi.org/10.1177/2053019614564785.

[4] G7. G7 Summit Declaration 2015. www.consilium.europa.eu/en/meetings/international-summit/2015/06/07-08/. Accessed on October 30, 2024.

[5] Ingarao G, Priarone PC. A comparative assessment of energy demand and life cycle costs for additive- and subtractive-based manufacturing approaches. J Manuf Process 2020;56:1219–29. https://doi.org/10.1016/j.jmapro.2020.06.009.

[6] Priarone PC, Ingarao G. Towards criteria for sustainable process selection: On the modelling of pure subtractive versus additive/subtractive integrated manufacturing approaches. J Clean Prod 2017;144:57–68. https://doi.org/10.1016/j.jclepro.2016.12.165.

[7] Song YS, Youn JR, Gutowski TG. Life cycle energy analysis of fiber-reinforced composites. Compos Part A Appl Sci Manuf 2009;40:1257–65. https://doi.org/10.1016/j.compositesa.2009.05.020.

[8] Jayal AD, Badurdeen F, Dillon OW, Jawahir IS. Sustainable manufacturing: Modeling and optimization challenges at the product, process and system levels. CIRP J Manuf Sci Technol 2010;2:144–52. https://doi.org/10.1016/j.cirpj.2010.03.006.

[9] Ellen MacArthur Foundation. Growth within: a circular economy vision for a competitive europe 2015. https://www.ellenmacarthurfoundation.org/assets/downloads/publications/EllenMacArthurFoundation_Growth-Within_July15.pdf. Accessed on October 30, 2024.

[10] Chen D, Heyer S, Ibbotson S, Salonitis K, Steingrímsson JG, Thiede S. Direct digital manufacturing: definition, evolution, and sustainability implications. J Clean Prod 2015;107:615–25. https://doi.org/10.1016/j.jclepro.2015.05.009.

[11] Duflou JR, De Moor J, Verpoest I, Dewulf W. Environmental impact analysis of composite use in car manufacturing. CIRP Ann - Manuf Technol 2009;58:9–12. https://doi.org/10.1016/j.cirp.2009.03.077.

[12] Naqvi SR, Prabhakara HM, Bramer EA, Dierkes W, Akkerman R, Brem G. A critical review on recycling of end-of-life carbon fibre/glass fibre reinforced composites waste using pyrolysis towards a circular economy. Resour Conserv Recycl 2018;136:118–29. https://doi.org/10.1016/j.resconrec.2018.04.013.

[13] Oliveux G, Dandy LO, Leeke GA. Current status of recycling of fibre reinforced polymers: Review of technologies, reuse and resulting properties. Prog Mater Sci 2015;72:61–99. https://doi.org/10.1016/j.pmatsci.2015.01.004.

[14] Zhang J, Chevali VS, Wang H, Wang C-H. Current status of carbon fibre and carbon fibre composites recycling. Compos Part B Eng 2020;193:108053. https://doi.org/10.1016/j.compositesb.2020.108053.

[15] Hyde JR, Lester E, Kingman S, Pickering S, Wong KH. Supercritical propanol, a possible route to composite carbon fibre recovery: A viability study. Compos Part A Appl Sci Manuf 2006;37:2171–5. https://doi.org/10.1016/j.compositesa.2005.12.006.

[16] Kennerley JR, Kelly RM, Fenwick NJ, Pickering SJ, Rudd CD. The characterisation and reuse of glass fibres recycled from scrap composites by the action of a fluidised bed process. Compos Part A Appl Sci Manuf 1998;29:839–45. https://doi.org/10.1016/S1359-835X(98)00008-6.

[17] Lunetto V, Galati M, Settineri L, Iuliano L. Unit process energy consumption analysis and models for Electron Beam Melting (EBM): Effects of process and part designs. Addit Manuf 2020;33:101115. https://doi.org/10.1016/j.addma.2020.101115.

[18] Kara S, Li W. Unit process energy consumption models for material removal processes. CIRP Ann - Manuf Technol 2011;60:37–40. https://doi.org/10.1016/j.cirp.2011.03.018.

[19] Kellens K, Baumers M, Gutowski TG, Flanagan W, Lifset R, Duflou JR. Environmental Dimensions of Additive Manufacturing: Mapping Application Domains and Their Environmental Implications. J Ind Ecol 2017;21:S49–68. https://doi.org/10.1111/jiec.12629.

[20] Gutowski T, Dahmus J, Thiriez A. Electrical energy requirements for manufacturing processes. Proc. 13th CIRP Int. Conf. Life Cycle Eng. LCE 2006, 2006, p. 623–8.

[21] Baffari D, Reynolds AP, Masnata A, Fratini L, Ingarao G. Friction stir extrusion to recycle aluminum alloys scraps: Energy efficiency characterization. J Manuf Process 2019;43:63–9. https://doi.org/10.1016/j.jmapro.2019.03.049.

[22] Lunetto V, Priarone PC, Galati M, Minetola P. On the correlation between process parameters and specific energy consumption in fused deposition modelling. J Manuf Process 2020;56:1039–49. https://doi.org/10.1016/j.jmapro.2020.06.002.

[23] Tiwari AS, Yang S. Energy Consumption Modeling of 3D-Printed Carbon-Fiber-Reinforced Polymer Parts. Polymers (Basel) 2023;15:1290. https://doi.org/10.3390/polym15051290.

[24] Katsiropoulos C V., Loukopoulos A, Pantelakis SG. Comparative Environmental and Cost Analysis of Alternative Production Scenarios Associated with a Helicopter's Canopy. Aerospace 2019;6:3. https://doi.org/10.3390/aerospace6010003.

[25] Witik RA, Gaille F, Teuscher R, Ringwald H, Michaud V, Månson JAE. Economic and environmental assessment of alternative production methods for composite aircraft components. J Clean Prod 2012;29–30:91–102. https://doi.org/10.1016/j.jclepro.2012.02.028.

[26] Granta Design. CES Selector Software (v.17.2.0 database) 2017. https://www.grantadesign.com/industry/products/ces-selector/.

[27] Suzuki T, Takahashi J. Prediction of energy intensity of carbon fiber reinforced plastics for mass-produced passenger cars. Ninth Japan Int SAMPE Symp JISSE-9 2005:14–9.

[28] Howarth J, Mareddy SSR, Mativenga PT. Energy intensity and environmental analysis of mechanical recycling of carbon fibre composite. J Clean Prod 2014;81:46–50. https://doi.org/10.1016/j.jclepro.2014.06.023.

[29] Office of Energy Efficiency & Renewable Energy. Bandwidth Study on Energy Use and Potential Energy Saving Opportunities in U.S. Glass Fiber Reinforced Polymer Manufacturing 2017:64. https://www.energy.gov/sites/prod/files/2019/05/f62/GFRP_bandwidth_study_2017.pdf . Accessed on October 30, 2024.

[30] Office of Energy Efficiency & Renewable Energy. Bandwidth Study on Energy Use and Potential Energy Saving Opportunities in U.S. Carbon Fiber Reinforced Polymer Manufacturing 2017:63. https://www.energy.gov/sites/default/files/2019/05/f62/CFRP_bandwidth_study_2017_0.pdf . Accessed on October 30, 2024.

[31] Pantelakis SG, Katsiropoulos CV, Labeas GN, Sibois H. A concept to optimize quality and cost in thermoplastic composite components applied to the production of helicopter canopies. Compos Part A Appl Sci Manuf 2009;40:595–606. https://doi.org/10.1016/j.compositesa.2009.02.012.

[32] Grouve WJB. Weld strength of laser-assisted tape-placed thermoplastic composites. University of Twente, 2012. https://doi.org/10.3990/1.9789036533928.

[33] Lunetto V, Galati M, Settineri L, Iuliano L. Sustainability in the manufacturing of composite materials : A literature review and directions for future research. J Manuf Process 2023;85:858–74. https://doi.org/10.1016/j.jmapro.2022.12.020.

[34] Ashby M. Materials and the Environment. second ed. Elsevier; 2013. https://doi.org/10.1016/C2010-0-66554-0.

[35] Liu W, Deng K, Wei H, Zhao P, Li J, Zhang Y. A decision-making model for comparing the energy demand of additive-subtractive hybrid manufacturing and conventional subtractive manufacturing based on life cycle method. J Clean Prod 2021;311:127795. https://doi.org/10.1016/j.jclepro.2021.127795.

[36] Liu W, Wei H, Zhang M, Luo Y, Zhang Y. Energy consumption modeling of additive-subtractive hybrid manufacturing based on cladding head moving state and deposition efficiency. Int J Adv Manuf Technol 2022;120:7755–70. https://doi.org/10.1007/s00170-022-09265-2.

[37] Nascimento DLM, Alencastro V, Quelhas OLG, Caiado RGG, Garza-Reyes JA, Rocha-Lona L, et al. Exploring Industry 4.0 technologies to enable circular economy practices in a manufacturing context. J Manuf Technol Manag 2019;30:607–27. https://doi.org/10.1108/JMTM-03-2018-0071.

[38] Wartbichler R, Clemens H, Mayer S, Ghibaudo C, Rizza G, Galati M, et al. On the Formation Mechanism of Banded Microstructures in Electron Beam Melted Ti–48Al–2Cr–2Nb and the Design of Heat Treatments as Remedial Action. Adv Eng Mater 2021;23. https://doi.org/10.1002/adem.202101199.

[39] Saade MRM, Yahia A, Amor B. How has LCA been applied to 3D printing? A systematic literature review and recommendations for future studies. J Clean Prod 2020;244:118803. https://doi.org/10.1016/j.jclepro.2019.118803.

[40] Ahmad N, Enemuoh EU. Energy modeling and eco impact evaluation in direct metal laser sintering hybrid milling. Heliyon 2020;6:e03168. https://doi.org/10.1016/j.heliyon.2020.e03168.

[41] Paris H, Mokhtarian H, Coatanéa E, Museau M, Ituarte IF. Comparative environmental impacts of additive and subtractive manufacturing technologies. CIRP Ann 2016;65:29–32. https://doi.org/10.1016/j.cirp.2016.04.036.

[42] Kumar S, Kruth J-P. Composites by rapid prototyping technology. Mater Des 2010;31:850–6. https://doi.org/10.1016/j.matdes.2009.07.045.

[43] Goh GD, Yap YL, Agarwala S, Yeong WY. Recent Progress in Additive Manufacturing of Fiber Reinforced Polymer Composite. Adv Mater Technol 2019;4:1–22. https://doi.org/10.1002/admt.201800271.

[44] Galati M, Viccica M, Minetola P. A finite element approach for the prediction of the mechanical behaviour of layered composites produced by Continuous Filament Fabrication (CFF). Polym Test 2021;98. https://doi.org/10.1016/j.polymertesting.2021.107181.

[45] Markforged. https://s3.amazonaws.com/mf.product.doc.images/Datasheets/Translations/IT/Markforged_CompositesV5.1_it.pdf. Accessed on October 30, 2024.

[46] Yi L, Ravani B, Aurich JC. Energy performance-oriented design candidate selection approach for additive manufacturing using toolpath length comparison method. Manuf Lett 2022;33:5–10. https://doi.org/10.1016/j.mfglet.2022.06.001.

[47] Ma Z, Gao M, Wang Q, Wang N, Li L, Liu C, et al. Energy consumption distribution and optimization of additive manufacturing. Int J Adv Manuf Technol 2021;116:3377–90. https://doi.org/10.1007/s00170-021-07653-8.

[48] Priarone PC, Catalano AR, Simeone A, Settineri L. Effects of deposition parameters on cumulative energy demand for Cold Metal Transfer additive manufacturing processes. CIRP Ann 2022;71:17–20. https://doi.org/10.1016/j.cirp.2022.03.022.

[49] Yi L, Glatt M, Thomas Kuo T-Y, Ji A, Ravani B, Aurich JC. A method for energy modeling and simulation implementation of machine tools of selective laser melting. J Clean Prod 2020;263:121282. https://doi.org/10.1016/j.jclepro.2020.121282.

[50] Ma Z, Gao M, Guo K, Wang Q, Li L, Liu C, et al. Analysis and Optimization of Energy Consumption for Multi-part Printing Using Selective Laser Melting and Considering the Support Structure. Int J Precis Eng Manuf Technol 2022. https://doi.org/10.1007/s40684-022-00450-y.

[51] Hu L, Wang Y, Shu L, Cai W, Lv J, Xu K. Energy benchmark for evaluating the energy efficiency of selective laser melting processes. Appl Therm Eng 2023;221:119870. https://doi.org/10.1016/j.applthermaleng.2022.119870.